

MODEL DEVELOPMENT FOR THE ESTIMATION OF URBAN AIR TEMPERATURE BASED ON SURFACE TEMPERATURE AND NDVI – A CASE STUDY IN SZEGED

Y GUO¹, T GÁL¹, G TIAN², H LI^{2,3} and J UNGER¹

¹*Department of Climatology and Landscape Ecology, University of Szeged, Egyetem u. 2., 6720 Szeged, Hungary
E-mail: guoyuchen@geo.u-szeged.hu*

²*College of Landscape Architecture and Art, Henan Agricultural University, Nongye str. 63., 450002 Zhengzhou, China*

³*Department of Landscape Planning and Regional Development, Szent István University, Villányi u. 29-43., 1118 Budapest, Hungary*

Summary: Predictive models for urban air temperature (T_{air}) were developed by using urban land surface temperature (LST) retrieved from Landsat-8 and MODIS data, NDVI retrieved from Landsat-8 data and T_{air} measured by 24 climatological stations in Szeged. The investigation focused on summer period (June–September) during 2016–2019 in Szeged. The relationship between T_{air} and LST was analyzed by calculating Pearson correlation coefficient, root-mean-square error and mean-absolute error using the data of 2017–2019, then unary (LST) and binary (LST and NDVI) linear regression models were developed for estimating T_{air} . The data in 2016 were used to validate the accuracy of the models. Correlation analysis indicated that there were strong correlations during the nighttime and relatively weaker ones during the daytime. The errors between T_{air} and $LST_{\text{MODIS-Night}}$ was the smallest, followed by $LST_{\text{MODIS-Day}}$ and $LST_{\text{Landsat-8}}$ respectively. The validation results showed that all models could perform well, especially during nighttime with an error of less than 1.5°C. However, the addition of NDVI into the linear regression models did not significantly improve the accuracy of the models, and even had a negative effect. Finally, the influencing factors and temporal and spatial variability of the correlation between T_{air} and LST were analyzed. $LST_{\text{Landsat-8}}$ had a larger original error with T_{air} , but the regression model based on Landsat-8 had a stronger ability to reduce errors.

Key words: Surface temperature, air temperature, NDVI, correlation and error analysis, predictive model, Szeged

1. INTRODUCTION

Urbanization is characterized by extensive land use transformation and altered surface thermal characteristics (Kalnay and Cai 2003, Shiflet et al. 2017). By changing the material and energy flows, urbanization has transformed the natural ecosystem to a coupled human and natural system, which inevitably has resulted in various effects on the eco-environment, including effects on the urban thermal environment, especially in urban regions having intensive population and high building density (Peng et al. 2016). One representative effect on the urban thermal environment is the appearance of urban heat island (UHI), a phenomenon where urban areas experience a higher temperature relative to their rural surroundings, especially at night (Oke 1987). There are two main approaches to quantify UHI including measurement of air temperature (T_{air}) in the canopy layer and land surface temperature (LST) (Schwarz et al. 2011, Sheng et al. 2017).

Due to the respective characteristics of these two types of temperature, the most common data sources used in studies on T_{air} and LST differ substantially (Oke et al. 2017,

Schwarz et al. 2012). For T_{air} collection, field measurements are generally used including fixed and mobile meteorological stations (Li et al. 2020, Unger et al. 2009). However, the limitation of number and uneven distribution of meteorological stations are serious shortcomings for T_{air} measurement in most urban areas, especially the lack of observations in densely built-up areas where the UHI effect is the strongest (Ho et al. 2016, Sheng et al. 2017); as for mobile measurement, in addition to the above problems, the accuracy of measurement is affected by the observation methodological design and route selection (Zhou et al. 2019). For LST data collection, the most common method is retrieving from satellite data (Tsou et al. 2017). Besides, infrared aircraft and camera are also used in some researches at local or street scale (Kelly et al. 1992, Unger et al. 2010). However, shortcomings still exist in these remote methods, such as limitation by weather conditions and observation frequency (Yang et al. 2020).

The interaction and correlation between urban T_{air} and LST have been proven in many studies (Roth et al. 1989, Schwarz et al. 2012), but it is worth noting that there are large differences between these two temperatures as a result of a high degree of spatial heterogeneity in thermal characteristics associated with urbanization (Prihodko and Goward 1997, Oke et al. 2017). In many studies on estimation of T_{air} based on remote sensing data, the T_{air} samples are scarce due to the lack of stations, and most of them are located in the suburbs far from the city centre, which cannot reflect the intra-urban air thermal environment exactly (Sheng et al. 2017, Pelta et al. 2016).

In our investigation, 24 meteorological stations, which were installed based on LCZs (Stewart and Oke 2012) and can represent all types of urban land covers in Szeged, were used to measure T_{air} (Unger et al. 2014). The objectives of our study are: (1) to analyse the connection between T_{air} and LST by using data from 2017 to 2019 and develop unary regression models for estimating T_{air} based on LST; (2) to validate the performance of the regression models by using data in 2016; (3) to add Normalised Difference Vegetation Index (NDVI) as the second independent variable to the regression models to develop binary regression models for T_{air} estimation and analyse the impact of NDVI on T_{air} ; (4) to analyse the influencing factors on the relationship between T_{air} and LST.

2. MATERIAL AND METHODS

2.1. Study area

We carried out our investigation in Szeged (46.3°N, 20.1°E), which is the largest city with a population of 162 000 in the southern region of the Great Hungarian Plain. The study area is a large flood plain and about 79 m above sea level. Tisza River passes through the city, but it is relatively narrow and its influence is negligible (Unger et al. 2001). This area is in Köppen's climatic region Cfa (Unger et al. 2020) with an annual mean temperature of 11.9°C, an amount of yearly precipitation of 508 mm, sunshine duration of 2049 hours and frequent drought (Harris et al. 2014). The study area covers a 10 km × 8 km rectangle in and around Szeged (Fig. 1).

2.2. Satellite data

In our study, LST were retrieved from Landsat-8 and MODIS. Our investigation focused on one season period from June to September during 4 years (2016–2019).

According to the weather condition, we selected 13 cloud free days to collect temperature data in Szeged region. Both Landsat-8 and MODIS are available in these 13 days. However, the data in some pixels of satellite images, especially at night, and some T_{air} obtained from meteorological stations are missing. After pairing LST with T_{air} , we got the final temperature data pairs (Table 1).

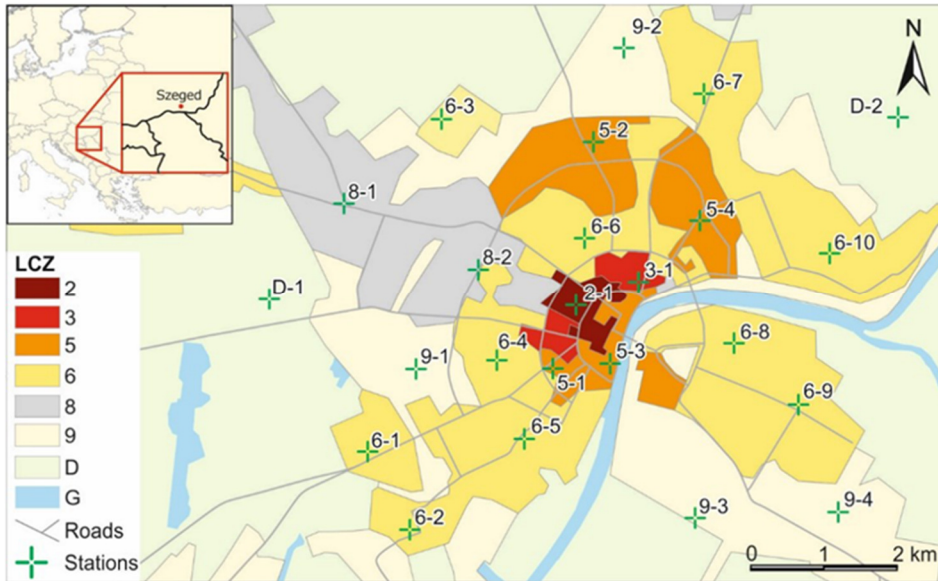


Fig. 1 Geographical location of Szeged and LCZs map of the study area with station sites of the urban meteorological network (marked by green crosses and digits referring to the zones) (Unger et al. 2018). For the explanation of LCZ classes see Stewart and Oke (2012).

Table 1 Information about the satellite data

Data source	Resolution	Observation time (UTC)	Amount of pairs of T_{air} and LST	
			2016	2017–2019
LST-Landsat-8	100 m	9:27	91	167
LST-MODIS-day	1000 m	10:54, 12:36	181	325
LST-MODIS-night	1000 m	1:30, 20:24	160	179
NDVI-Landsat-8	30 m	9:27	91	167

All processing and calculations of satellite data were carried out in Google Earth Engine (GEE) platform. GEE is a cloud computing platform designed to store and process huge data sets (at petabyte-scale) for analysis and ultimate decision making (Kumar and Mutanga 2018). Following the free availability of Landsat series in 2008, Google archived all the data sets and linked them to the cloud computing engine for open source use. The current archive of data includes those from other satellites, as well as Geographic Information Systems (GIS) based vector data sets, social, demographic, weather, digital elevation models, and climate data layers (Mutanga and Kumar 2019). The LST retrieval process was performed in the background on the Google cloud computing servers, with direct access to the GEE satellite data catalogue. Therefore, the application needs only a few seconds to produce Landsat-8 LST with no need for any computational resources from the user

(Parastatidis et al. 2017). In our investigation, the applications of GEE include LST retrieval from Landsat-8 and MODIS datasets, calculation of Normalized Difference Vegetation Index (NDVI) with Landsat-8 data and distance-weighted average calculation of LST and NDVI. All of the images were projected to UTM zone 34N and keep their original resolution.

(1) NDVI

NDVI image shows the vegetation extent of the area by analysing near-infrared and red spectral band data. NDVI is the index of photosynthetic activity in plant and it is the most commonly used vegetation spectral indices for crop growth monitoring (Pirotti et al. 2014). In this research, the purposes of calculating NDVI are: (1) to calculate the land surface emissivity (τ) for LST retrieval from Landsat-8 (Molnár 2016); (2) to create the binary regression model for T_{air} estimate. As the resolution of Landsat-8 (30 m) is higher than MODIS (250 m – 1 km), NDVI was calculated with Landsat-8 data according to the following equation (Tucker 1979):

$$NDVI = \frac{b5 - b4}{b5 + b4}$$

where b5 is the reflectance of near-infrared band and b4 is the reflectance of red band in Landsat-8 dataset.

(2) LST retrieval from satellite data

The Radiative Transfer Equation method was used to retrieve LST from Landsat-8 data. In this method, the main task is removing the atmospheric attenuation effects and calculation of land surface emissivity (Yu et al. 2014). The atmospheric profile was extracted from NASA's Atmospheric Correction Parameter Calculator (Barsi et al. 2003), which uses the National Centres for Environmental Prediction modeled atmospheric global profiles for a particular date, time and location as input. Then, the Moderate Resolution Atmospheric Transmission model was used to simulate atmospheric transmittance, upwelling and downwelling. The whole process can be expressed as the following equations:

$$L_{\lambda} = [\varepsilon B(T_s) + (1 - \varepsilon)L_{\downarrow}] \tau + L_{\uparrow}$$

$$B(T_s) = \frac{[L_{\lambda} - L_{\uparrow} - \tau(1 - \varepsilon)L_{\downarrow}]}{\tau \varepsilon}$$

where L_{λ} is the at-sensor radiance, L_{\uparrow} is the upwelling atmospheric radiance, L_{\downarrow} is the downwelling atmospheric radiance in $Wm^{-2}sr^{-1}\mu m^{-1}$, τ is the total atmospheric transmissivity between the surface and the sensor, and ε is the land surface emissivity, which can be calculated based on NDVI (Qin et al. 2004, Sobrino et al. 2004), $B(T_s)$ is the radiance of a blackbody target of kinetic temperature T_s in $Wm^{-2}sr^{-1}\mu m^{-1}$. Then an inversion of Planck's Law was applied to derive the kinetic skin temperature using the following equation:

$$T_s = \frac{K_2}{\ln \frac{K_1}{B(T_s) + 1}}$$

where K_1 and K_2 are the thermal band calibration constants found in the Landsat-8 metadata files ($K_1=774.89$, $K_2=1321.08$).

As for MODIS data, the daily LST and Emissivity products were used over Szeged. The version-5 products from 2016 to 2019 were collected for this study, which are abbreviated as MOD11A1 and MYD11A1 and have a spatial resolution of approximately 1 km (Sun et al. 2015, Wan 2008). MODIS data were collected by both the Terra and Aqua Sun-synchronous satellites. Terra passes the equator from north to south (descending node) at approximately 10:30 a.m. and Aqua passes the equator from south to north (ascending node) at approximately 1:30 p.m. local time. The land-surface thermal radiation can be obtained at least four times each day in our study area. Nevertheless, there are some areas without LST data in MODIS images, especially at night, so the final daytime data is twice the night-time data. The details of NDVI and both LSTs from Landsat-8 and MODIS are shown in Table 1.

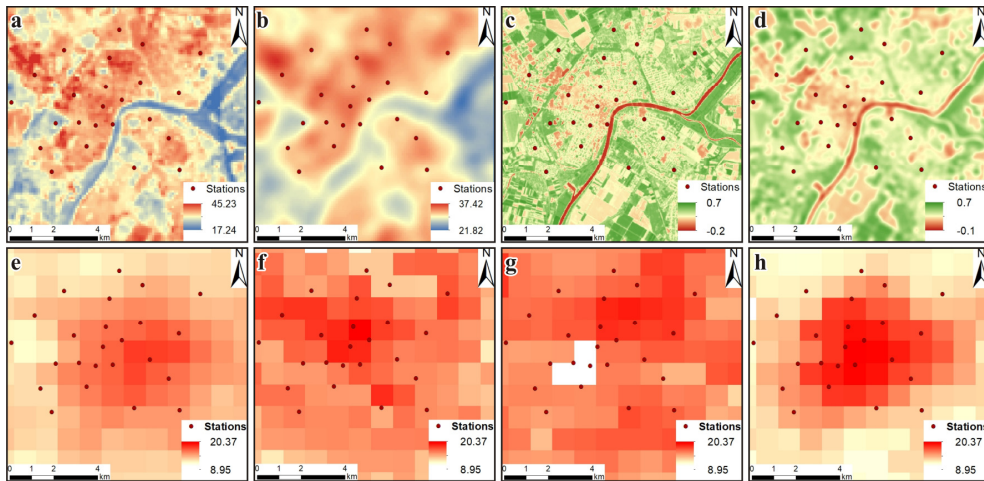


Fig. 2 Examples of spatial patterns of LST and NDVI: (a) and (c) LST and NDVI from Landsat-8, 2017-06-24, 9:27 (UTC), respectively; (e–h) LST from MODIS MOD11A1 and MYD11A1, 2016-07-07, 1:30, 10:54, 12:36 and 20:24 (UTC), respectively; (b) and (d) distance-weighted average of LST and NDVI, respectively

(3) Distance-weighted average

MODIS and Landsat-8 images have different spatial resolutions. Therefore, to be comparable and usable in statistical analysis, the distance-weighted spatial average of NDVI and $LST_{Landsat-8}$ was calculated. As shown in Figs. 2b and d, the value in each pixel is the distance-weighted average of all pixel in a 1 km square centered this pixel (Unger et al. 2009). Considering that the T_{air} is affected by LST and air turbulence and these influence factors on T_{air} at 4 m height may extend over a local scale, hence it is reasonable to choose the range of 1 km to calculate the spatial average LST. This calculation process was carried out in GEE. As for the MODIS data, we used the original value (Fig. 2).

2.3. T_{air} data collection

T_{air} data were obtained from a meteorological monitoring network in Szeged. This monitoring network was established in Szeged within the framework of an EU project (URBAN-PATH 2016, urban-path.hu). 24 stations were installed to measure T_{air} and relative humidity every 10 minutes. The locations of the stations were selected based on the distribution of LCZs in Szeged (Lelovics et al. 2014, Unger et al. 2018). All of stations have to be representative of the LCZs within the city and spatial pattern of the network has to be capable of revealing the spatial structure of the UHI (Unger et al. 2015). The accuracy of the thermal sensors is 0.4°C. The consoles are mounted on lamp posts at the height of 4 m above the ground for security reasons. As the air in the urban canyon is well-mixed, the temperature measured at this height is representative of the lower air layers (Nakamura and Oke 1988, Unger et al. 2014). When we paired T_{air} with LST, if their observation time was not exactly synchronous, we chose the closest T_{air} to the LST with the temporal interval of less than five minutes (Gál et al. 2016).

2.4. Methods of statistical analysis

Statistical analysis was performed by SPSS 25.0 and Microsoft Excel 2019. Correlation, error and regression analysis were employed in this study. Pearson correlation coefficient (r) was computed to evaluate the correlation between LST and T_{air} . Root-mean-square error (RMSE) and mean-absolute error (MAE) were computed to quantitatively evaluate the difference between LST and T_{air} . Then, linear regression models were created to estimate T_{air} based on LST and NDVI during 2017–2019. Finally, the T_{air} , LST and NDVI data in 2016 were used to validate the performance of these models. For this validation, the RMSE and MAE between estimated T_{air} and measured T_{air} were calculated and compared (Janssen and Heuberger 1995, Hrisko et al. 2020). The unary and binary regression models are shown as the following equations:

$$T_{\text{air}}=a \cdot \text{LST}+e$$

$$T_{\text{air}}=a \cdot \text{LST}+b \cdot \text{NDVI}+e$$

3. RESULTS

3.1. Connection and error analysis between T_{air} and LST

Relationships between T_{air} and LST over 9-day periods from 2017 to 2019 were calculated using 671 data pairs (Fig. 3). As error analyse (RMSE and MAE) shows (Fig. 3 a–c), errors between T_{air} and $\text{LST}_{\text{Landsat-8}}$ were largest with an RMSE of 6.1°C and an MAE of 5.6°C, and the errors between T_{air} and $\text{LST}_{\text{MODIS-Day}}$ were relatively smaller with an RMSE of 4.2°C and an MAE of 3.6°C, the smallest errors (RMSE=2.3°C and MAE=2.0°C) appear at night when $\text{LST}_{\text{MODIS-Night}}$ were used to compare with T_{air} . In Pearson’s correlation analysis, the stronger connection between T_{air} and LST appears at night ($\text{LST}_{\text{MODIS-Night}}$, $r=0.97$, $P<0.01$) compared with $\text{LST}_{\text{Landsat-8}}$ ($r=0.89$, $P<0.01$) and $\text{LST}_{\text{MODIS-Day}}$ ($r=0.89$, $P<0.01$). In general, the difference between T_{air} and LST varies from day to night; T_{air} has a stronger connection and smaller errors with LST at night. When the influence of solar radiation ceases, the energy exchange between air and surface tends to be stable at night; the difference

between T_{air} and LST decreases and the correlation increases significantly, which is the same as the results of previous studies (e.g. Sun et al. 2015). $LST_{MODIS-Day}$ has the same connection but smaller errors with T_{air} compared with $LST_{Landsat-8}$, which may be caused by the inherent differences between these two data sources and their different observation time.

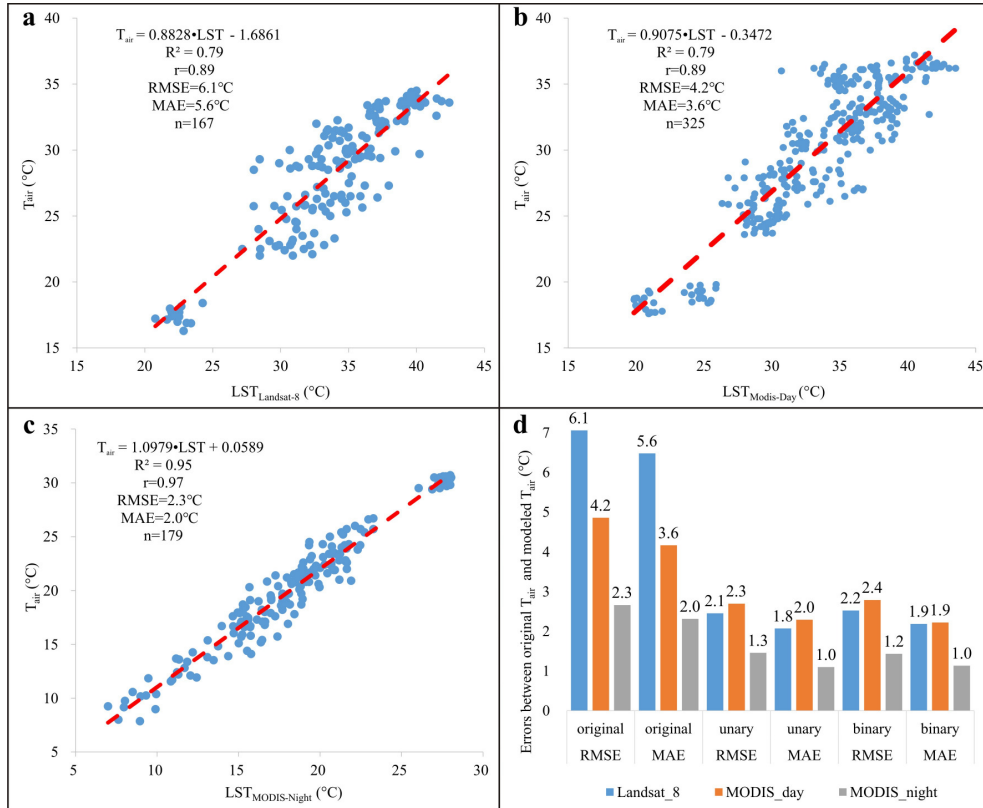


Fig. 3 (a), (b) and (c): Results of regression, correlation and error analysis between T_{air} and $LST_{Landsat-8}$, $LST_{MODIS-Day}$ and $LST_{MODIS-Night}$, respectively, from 2017 to 2019; (d): The error analysis between observed T_{air} and estimated T_{air} in 2016

3.2. Development and validation of regression models

The differences between T_{air} and LST are obvious and unignored, despite their moderate to high correlation. So we trained regression models based on T_{air} and LST data during 2017–2019 to estimate T_{air} (Fig. 3a–c). The results showed that the value of R^2 was 0.79 ($P < 0.01$) when $LST_{Landsat-8}$ and $LST_{MODIS-Day}$ were used in models, which means 79% of the variation of T_{air} can be explained by the LST. In addition, the night-time model, with a higher R^2 of 0.97 ($P < 0.01$), can perform better than that during daytime, which means almost all of the variation of T_{air} can be explained by the LST. Then, these regression equations were validated by using the LST data in 2016. We estimated T_{air} basing on $LST_{Landsat-8}$ and LST_{MODIS} in 2016 and calculated the RMSE and MAE between real T_{air} and estimated T_{air} (Fig. 3d). The results indicated that all models could reduce the error to less than 2.5°C,

especially when $LST_{MODIS-Night}$ were used in the model with an RMSE of $1.3^{\circ}C$ and MAE of $1.0^{\circ}C$, which means that T_{air} can be accurately estimated using only LST at night.

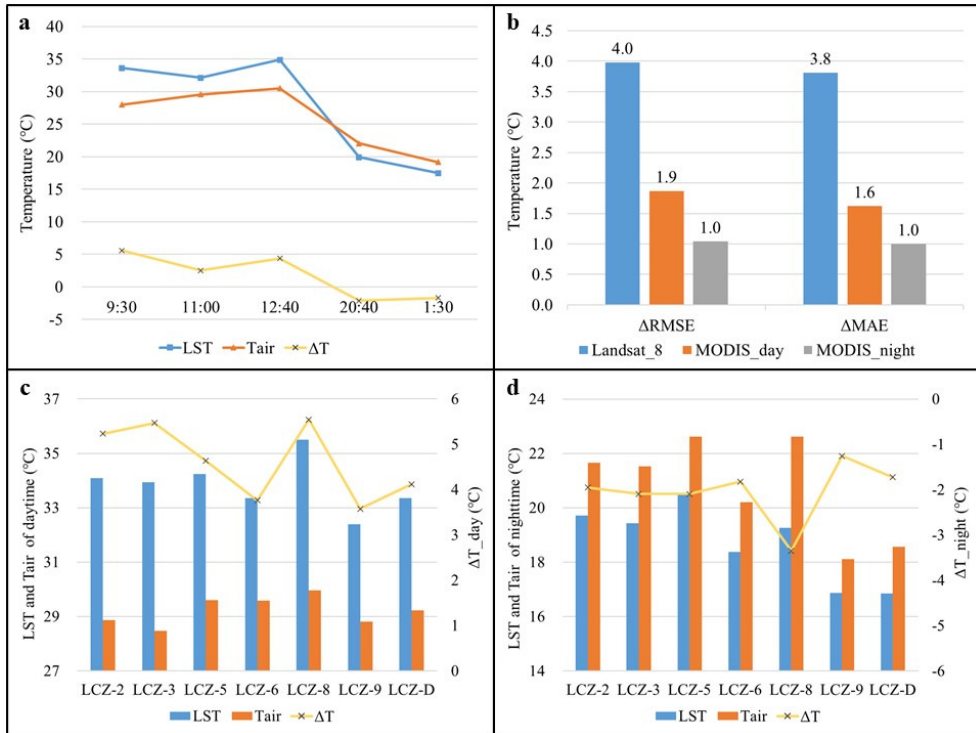


Fig. 4 (a) Average of LST, T_{air} and the difference between LST and T_{air} (ΔT) at 5 observation time (9:30, 11:00, 12:40, 20:40 and 1:30); (b) The difference between original errors and estimated errors; (c) and (d): Mean value of T_{air} , LST and temperature difference (ΔT) between T_{air} and LST by LCZs during daytime and nighttime, respectively

In consideration of the effect of vegetation on the urban thermal environment (Shiflett et al. 2017), we tried to add NDVI into the regression models to develop binary regression models. The coefficients of determination (R^2) of models based on $LST_{Landsat-8}$, $LST_{MODIS-Day}$ and $LST_{MODIS-Night}$ were 0.80, 0.80 and 0.95 ($P < 0.01$), respectively, which means that these models can effectively estimate T_{air} . In order to compare with unary regression models, we calculated the RMSE and MAE between observed T_{air} and estimated T_{air} based on both models without and with NDVI (Fig. 3d). Unexpectedly, we saw a slight increase in errors when binary regression models were used, only $RMSE_{MODIS-Night}$ and $MAE_{MODIS-Day}$ decreased from $1.3^{\circ}C$ to $1.2^{\circ}C$ and from $2.0^{\circ}C$ to $1.9^{\circ}C$, respectively. This results indicate that the role of urban vegetation may not be important for estimating T_{air} .

4. DISCUSSION

4.1 Comparison of Landsat-8 and MODIS

The results of Section 3.1 showed that T_{air} had the same connection with $LST_{\text{Landsat-8}}$ as with $LST_{\text{MODIS-Day}}$. However, it should be noted that errors between T_{air} and $LST_{\text{Landsat-8}}$ are obviously higher than errors between T_{air} and LST_{MODIS} , which is mainly the result of high $LST_{\text{Landsat-8}}$. We calculated the average of LST, T_{air} and the difference between LST and T_{air} (ΔT) at 5 observation time (9:30, 11:00, 12:40, 20:40 and 1:30, Fig. 4a). When Landsat-8 was used to retrieve LST (9:30), the average $LST_{\text{Landsat-8}}$ was relatively higher than the average LST_{MODIS} at 11:00, which was inconsistent with the fluctuation of T_{air} . This differential can be explained by the inherent error between Landsat-8 data and MODIS data, which caused the highest ΔT , RMSE and MAE at 9:30.

We also compared the performance of regression models based on $LST_{\text{Landsat-8}}$, $LST_{\text{MODIS-Day}}$ and $LST_{\text{MODIS-Night}}$ by calculating $\Delta RMSE$ and ΔMAE (Fig. 4b). We found that the model based on $LST_{\text{Landsat-8}}$ could reduce the errors by nearly 4°C, which was the largest among these three values presented. Furthermore, the errors based on $LST_{\text{Landsat-8}}$ were smaller than that based on $LST_{\text{MODIS-Day}}$ after regression calculating (Fig. 3d), indicating that Landsat-8 data can perform better than MODIS-Day data in T_{air} estimation. On the one hand, the larger difference between $LST_{\text{Landsat-8}}$ and T_{air} caused the possibility of larger $\Delta RMSE$ and ΔMAE ; on the other hand, the climatological stations were not accurately located in the center of each pixel as a result of the wide pixel range of MODIS images, which caused a spatial error between T_{air} and LST_{MODIS} . This spatial error likely caused the differential of performance of estimation models based on MODIS-Day and Landsat-8 data.

4.2 Spatio-temporal variability of T_{air} and LST

As mentioned in Section 2, all 24 climatological stations are located in specific LCZs which are distinguished based on the characteristics of land surface (Lelovics et al. 2014, Unger et al. 2018). We calculated the mean value of T_{air} , LST and temperature difference (ΔT) between T_{air} and LST in each specific LCZ. As shown in Fig. 4c and 4d, the difference of LSTs among these LCZs were distinct, which indicated that the spatial variability of LST was greater than T_{air} during daytime. According to Oke et al. (2017), the variability in geometric, radiative, thermal, moisture and aerodynamic properties of urban surface underlie the greater spatial variability of LST compared to T_{air} , particularly during daytime. At that time, the most dominant surfaces with relatively high LST are roads, residential and industrial areas, etc. which are covered by artificial pavements, such as LCZs 2, 3 and 8. These areas are characterized by higher thermal conductivity and heat capacity, and in addition, there is less evaporative cooling effect over these surfaces. The influencing factors on T_{air} are different from the ones on LST. T_{air} is mainly affected by radiation, conduction and convection. During daytime, T_{air} is characterized by relatively high homogeneity as a result of country breeze and local airflow (Beranová and Huth 2005), which usually causes UHI to decline or even disappear. At night, T_{air} has a similar spatial variability to LST when country breeze and local airflow weaken and longwave radiation of surface dominates. Because of the spatial variability of T_{air} and LST, the spatial variability of ΔT is also obvious.

5. CONCLUSIONS

This study utilized Landsat-8 data and MODIS data to retrieve urban land surface temperature (LST) and measured urban air temperature (T_{air}) by 24 climatological stations in the period of 2016–2019 in Szeged. We compared LST and T_{air} by using error and connection analysis, then we developed and validated regression equations for estimating T_{air} based on LST, NDVI and T_{air} . Finally, by calculating the mean of LST, T_{air} and their difference at specific observation time and LCZ, we analysed the influencing factors on the relationship between T_{air} and LST. Based on our research results, we conclude:

(1) T_{air} and LST have a strong enough correlation during both day and night. The correlation at night is stronger ($r=0.97$) with lower errors (RMSE=2.3°C and MAE=2.0°C) and better regression model performance ($R^2=0.95$, $P<0.01$);

(2) All regression models can effectively estimate T_{air} , especially at night. The errors can be reduced below 2.5°C during the day and below 1.5°C at night. NDVI cannot enhance the performance of the T_{air} prediction models. On the contrary, a slight weakening can be observed when NDVI was added in models;

(3) The difference between $LST_{\text{Landsat-8}}$ and LST_{MODIS} is obvious in T_{air} estimation, which indicated that we should consider this difference when combining different satellite data. The difference in the temporal and spatial resolution of satellite imagery, as well as certain weather conditions, are limitations on the use of remote sensing data;

(4) The relationship between LST and T_{air} has obvious spatial and temporal variability. LST is higher than T_{air} during daytime, and the opposite is true at night. The difference between T_{air} and LST is relatively high in LCZs 2, 3 and 8 with more artificial surfaces.

Overall, in our study, 24 climatological stations distributed in 7 LCZs were used in and around urban area of Szeged, which is our advantage in T_{air} estimate compared with other studies. The models developed for estimating T_{air} make it possible to use LST as a substitute for T_{air} measurement in cities without enough climatological station.

Acknowledgement: This paper was supported by Stipendium Hungaricum Programme founding by the Hungarian Government.

REFERENCES

- Barsi JA, Barker JL, Schott JR (2003) An atmospheric correction parameter calculator for a single thermal band earth-sensing instrument. 2003 IEEE International Geoscience and Remote Sensing Symposium, Toulouse, France. 3014-3016
- Beranová R, Huth R (2005) Long-term changes in the heat island of Prague under different synoptic conditions. *Theor Appl Climatol* 82:113-118
- Gál T, Skarbit N, Unger J (2016) Urban heat island patterns and their dynamics based on an urban climate measurement network. *Hung Geogr Bull* 65:105-116
- Harris I, Jones PD, Osborn TJ, Lister DH (2014) Updated high-resolution grids of monthly climatic observations – the CRU TS3.10 Dataset. *Int J Climatol* 34:623-642
- Ho H, Knudby A, Xu Y, Hodul M, Aminipouri M (2016) A comparison of urban heat islands mapped using skin temperature, air temperature, and apparent temperature (Humidex), for the greater Vancouver area. *Sci Total Environ* 544: 929-938
- Hrisko J, Ramamurthy P, Yu Y, Yu P, Vázquez D (2020) Urban air temperature model using GOES-16 LST and a diurnal regressive neural network algorithm. *Rem Sens Environ* 237:111495
- Janssen PH, Heuberger PS (1995) Calibration of process-oriented models. *Ecol Model* 83:55-66

Model development for the estimation of urban air temperature based on surface temperature and NDVI – a case study in Szeged

- Kelly RB, Smith EA, MacPherson JI (1992) A comparison of surface sensible and latent heat fluxes from aircraft and surface measurements in FIFE 1987. *J Geophys Res* 97:18445-18453
- Kalnay E, Cai M (2003) Impact of urbanization and land-use change on climate. *Nature* 423:528-531
- Kumar L, Mutanga O (2018) Google Earth Engine applications since inception: usage, trends, and potential. *Rem Sens-Basel* 10:1509
- Lelovics E, Unger J, Gál T, Gál CV (2014) Design of an urban monitoring network based on Local Climate Zone mapping and temperature pattern modelling. *Clim Res* 60:51-62
- Li H, Meng H, He R, Lei Y, Guo Y, Ernest A, Jombach S, Tian G (2020) Analysis of cooling and humidification effects of different coverage types in Small Green Spaces (SGS) in the context of urban homogenization: A case of HAU Campus green spaces in summer in Zhengzhou, China. *Atmosphere* 11:862
- Molnár G (2016) Analysis of land surface temperature and NDVI distribution for Budapest using Landsat 7 ETM+ data. *Acta Climatol* 49-50:49-61
- Mutanga O, Kumar L (2019) Google Earth Engine applications. *Rem Sens-Basel* 11:591
- Nakamura Y, Oke TR (1988) Wind, temperature and stability conditions in an east–west oriented urban canyon. *Atmos Environ* 22: 2691-2700
- Oke TR (1987) *Boundary Layer Climates*. Methuen, London
- Oke TR, Mills G, Voogt JA (2017) *Urban Climates*. University Press, Cambridge
- Parastatidis D, Mitraka Z, Chrysoulakis N, Abrams M (2017) Online global land surface temperature estimation from Landsat. *Rem Sens-Basel* 9:1208
- Pelta R, Chudnovsky A, Schwartz J (2016) Spatio-temporal behavior of brightness temperature in Tel-Aviv and its application to air temperature monitoring. *Environ Poll* 208:153-160
- Peng J, Xie P, Liu Y, Ma J (2016) Urban thermal environment dynamics and associated landscape pattern factors: A case study in the Beijing metropolitan region. *Rem Sens Environ* 173:145-155
- Pirotti F, Parraga MA, Stuardo E, Dubbini M, Masiero A, Ramanzin M (2014) NDVI from Landsat 8 vegetation indices to study movement dynamics of Capra ibex in mountain areas. In: *ISPRS Technical Commission VII Symposium, XL-7:147-153*
- Prihodko L, Goward S (1997) Estimation of air temperature sensed surface observations. *Rem Sens Environ* 60:335-346
- Qin Z, Li W, Xu B, Zhang W (2004) Estimation method of land surface emissivity for deriving land surface temperature from Landsat TM6 data. *Adv Marine Sci* 22:129-137
- Roth M, Oke TR, Emery WJ (1989) Satellite-derived urban heat islands from three coastal cities and the utilization of such data in urban climatology. *Int J Rem Sens* 10:1699-1720
- Schwarz N, Schlink U, Franck U, Großmann K (2012) Relationship of land surface and air temperatures and its implications for quantifying urban heat island indicators – An application for the city of Leipzig (Germany). *Ecol Indic* 18:693-704
- Sheng L, Tang X, You H, Gu Q, Hu H (2017) Comparison of the urban heat island intensity quantified by using air temperature and Landsat land surface temperature in Hangzhou, China. *Ecol Indic* 72:738-746
- Shiflett S, Liang L, Crum S, Feyisa G, Wang J, Jenerette G (2017) Variation in the urban vegetation, surface temperature, air temperature nexus. *Sci Total Environ* 579:495-505
- Sobrino JA, Jiménez-Muñoz JC, Paolini L (2004). Land surface temperature retrieval from LANDSAT TM 5. *Rem Sens Environ* 90: 434-440
- Stewart ID, Oke TR (2012) Local Climate Zones for urban temperature studies. *Bull Am Meteorol Soc* 93:1879-1900
- Sun H, Chen Y, Zhan W (2015) Comparing surface- and canopy-layer urban heat islands over Beijing using MODIS data. *Int J Rem Sens* 36: 5448-5465
- Tsou J, Zhuang J, Li Y, Zhang Y (2017) Urban heat island assessment using the Landsat 8 data: A case study in Shenzhen and Hong Kong. *Urban Sci* 1:10-31
- Tucker C J (1979) Red and photographic infrared linear combinations for monitoring vegetation. *Rem Sens Environ* 8:127-150
- Unger J, Sümeghy Z, Gulyás Á, Bottyán Z, Mucsi L (2001) Land-use and meteorological aspects of the urban heat island. *Meteorol Appl* 8:189-194
- Unger J, Gál T, Rakonczai J, Mucsi L, Szatmári J, Tobak Z, Leeuwen B, Fiala K (2009). Air temperature versus surface temperature in urban environment. In: *The 7th International Conference on Urban Climate, Yokohama, Japan*
- Unger J, Gál T, Rakonczai J, Mucsi L, Szatmári J, Tobak Z, Leeuwen B, Fiala K (2010) Modeling of the urban heat island pattern based on the relationship between surface and air temperatures. *Időjárás* 114:287-302

- Unger J, Savic SM, Gál T, Milosevic DD (2014) Urban climate and monitoring network system in European cities. University of Novi Sad, University of Szeged, Novi-Sad, Szeged
- Unger J, Gál T, Csépe Z, Lelovics E, Gulyás Á (2015) Development, data processing and preliminary results of an urban human comfort monitoring and information system. *Időjárás* 119:337-354
- Unger J, Skarbit N, Gál T (2018) Absolute moisture content in mid-latitude urban canopy layer, part 2: results from Szeged, Hungary. *Acta Climatol* 51-52:47-56
- Unger J, Skarbit N, Kovács A, Gál T (2020) Comparison of regional and urban outdoor thermal stress conditions in heatwave and normal summer periods: A case study. *Urban Clim* 32:100619
- Wan Z (2008) New refinements and validation of the MODIS land-surface temperature/emissivity products. *Rem Sens Environ* 112:59-74
- Yang C, Yan F, Zhang S (2020) Comparison of land surface and air temperatures for quantifying summer and winter urban heat island in a snow climate city. *J Environ Manage* 265:110563
- Yu X, Guo X, Wu Z (2014) Land surface temperature retrieval from Landsat 8 TIRS – Comparison between Radiative Transfer Equation-Based Method, Split Window Algorithm and Single Channel Method. *Rem Sens-Basel* 6:9829-9852
- Zhou B, Kaplan S, Peeters A, Kloog I, Erell E (2019) “Surface,” “satellite” or “simulation”: Mapping intra-urban microclimate variability in a desert city. *Int J Climatol* 40:3099-3117